Int. J. Electrochem. Sci., 10 **(2015)** 8993 - 9005

International Journal of
ELECTROCHEMICAL
SCIENCE
www.electrochemsci.org

High Volumetric Energy Density Lithium Ion Battery with Titania@Carbon Nanostructure Electrode

Min-Cheol Kim[1, †], *Young-Woo Lee*[1,2, †], *Si-Jin Kim*[a], *Da-Hee Kwak*[1], *Han-Chul Park*[1], *Da-Mi Kim*[1], *and Kyung-Won Park*[1,*]

[1] Department of Chemical Engineering, Soongsil University, Seoul 156-743, Republic of Korea
[2] Department of Engineering Science, University of Oxford, Oxford OX1 3PJ, United Kingdom
[†] These authors contributed equally to this work.
[*]E-mail: kwpark@ssu.ac.kr

Received: 13 August 2015 / *Accepted:* 4 September 2015 / *Published:* 30 September 2015

In typical lithium ion batteries, anodes mainly contained active materials, a binder such as polyvinylidene fluoride (PVDF), and a conducting agent such as Ketjen black. In this study, we proposed a conducting agent-free electrode structure (f-TiO_2@C) fabricated using TiO_2@C, as an active material, with graphitic-like carbon shells and PVDF in the absence of the conducting material. For comparison, a conventional electrode (c-TiO_2@C) was fabricated using TiO_2@C and PVDF with the conducting material. In addition, the conducting agent-free and conventional electrode structures were prepared using TiO_2, as an active material, heated at 800 ^oC in air atmosphere. The high discharge capacity and enhanced high rate cycling performance of the f-TiO_2@C were attributed to the carbon shell in the TiO_2@C, which might play a role as an efficient conducting agent for the high-performance lithium ion batteries. Furthermore, the f-TiO_2@C as a conducting agent-free electrode exhibited much enhanced volumetric capacity and cycle life compared to the c-TiO_2@C in the presence of 10 wt% Ketjen black as a conducting agent.

Keywords: Conducting agent free, TiO_2, Graphitic-like carbon, Core-shell, lithium ion battery

1. INTRODUCTION

Lithium ion batteries (LIBs) have been considered as a promising energy storage device for various electric vehicles, energy storage systems, and other electric utilities.[1-8] In LIBs, the carbon-based materials as an anode having an improved electrical conductivity and high capacitance exhibit a lower voltage and higher capacity than the cathodes.[9-11] Compared with graphite, which has been typically used as an anode in LIBs, transition metal oxides have been studied as anode alternatives due

to their high theoretical capacities and high packing densities, resulting in high specific energy densities in the LIBs.[12-15]

Among the transition metal oxides, titanium oxide (TiO_2) has attracted considerable interest due to the earth abundance of elements, safe cell operation, and small volume expansion during lithium insertion/deinsertion.[16-22] However, to overcome the poor electrical conductivity and low Li-ion diffusion coefficient in TiO_2 as an anode of LIBs, intensive research has focused on the design of the TiO_2 electrodes in terms of size and structure. Strategies to improve the performance of the active materials include the reduced dimension of particles for an enhanced lithium ion diffusivity and carbon coating on active materials to increase electronic conductivity.[23-28] In particular, anode composite materials based on TiO_2 and carbon have exhibited excellent LIB performances due to the improved electronic and ionic transport.[29-35] The uniform and thin carbon layer coated on the TiO_2 in the nanocomposites can enable the particles to conduct electrons, which penetrate easily through the carbon layer into TiO_2 as an active electrode, resulting in high volumetric energy density and high rate performance.[36-41]

In this study, we prepared a nanocomposite based on TiO_2 and carbon as an anode for LIBs formed by heating TiO_2 at 800 °C in CH_4. The as-prepared nanocomposite was characterized using field-emission transmission electron microscopy (FE-TEM), field-emission scanning electron Microscope (FE-SEM), X-ray diffraction (XRD), Raman spectroscopy, and thermogravimetric analysis (TGA). To evaluate the LIB performance, we proposed a conducting agent-free electrode structure fabricated using an active material and binder in the absence of a conducting material. The charge-discharge and high-rate cycling curves and cyclic voltammograms (CVs) of the electrode were measured using a lithium coin cell.

2. EXPERIMENT PART

2.1 Materials synthesis

The nanocomposite was prepared by heating TiO_2 powder (Degussa, P-25) at 800 ^oC under a CH_4 atmosphere. At a CH_4 flow rate of 100 mL min^{-1}, the sample was heated from 25 ^oC to 800 ^oC and then maintained at 800 ^oC for 3h. For comparison with the nanocomposite, the electrode (TiO_2-800) was prepared by heating the TiO_2 powder at 800 ^oC for 3h in an air atmosphere.

2.2 Materials characterization

The morphology and size of the as-prepared samples were characterized by FE-TEM (Tecnai G2 F30 system operating at 300 kV). The FE-TEM samples were prepared by dropping the powder suspension with ethanol on a copper grid substrate. For the structural analysis of the electrodes, XRD analysis was performed using a Rigaku X-ray diffractometer with a Cu Kα (λ = 0.15418 nm) source with a Ni filter. The source was operated at 40 kV and 100 mA. For all XRD measurements, the resolution in the scans was kept at 0.02°. The 2θ between 20° and 60° was explored at a scan rate of 4^o

min^{-1}. The cross section thickness of the electrodes was measured using a field emission scanning electron microscopy (FE-SEM JSM-6700F). Raman spectra were recorded on a high resolution Micro-Raman spectrometer (LabRAM HR UV/Vis/NIR PL, Ar ion laser with $\lambda = 514.5$ nm). The TGA curve was measured in a thermal analyzer (SDT Q-600, TA Instruments) in the range of 25-800 ^oC at a heating rate of 10 $^oC\ min^{-1}$ in an air flow of 60 $cm^3\ min^{-1}$.

2.3 Electrochemical measurement

The anodes as an active material for LIBs were prepared by mixing TiO_2@C or TiO_2-800 and polyvinylidene fluoride (PVDF) as a binder with and without Ketjen black as a conducting agent. For the preparation of the slurry, several drops of N-methyl-pyrrolidone were added to the mixture of the as-prepared samples, Ketjen black and PVDF. The prepared slurry was homogeneously mixed by stirring and then uniformly coated on copper foils. The electrodes with an area of 1.3273 cm^2 were dried at 110 ^oC in a vacuum oven. The electrical conductivity of the as-prepared electrodes was measured in terms of the equation (1):

$$\sigma = 1/\rho = l/RA \quad (1)$$

where σ is the electrical conductivity (S cm^{-1}), ρ is the specific resistance, l is the thickness of the pellet, R is the resistance, and A is the area of the pellet.

The coin cells were assembled in a high purity argon filled glove box using the as-prepared electrodes as a working electrode, lithium foil (FMC Co.) as a counter electrode, and a separator that was saturated with the electrolyte solution that consisted of 1.1 M $LiPF_6$ dissolved in a solvent mixture (Techno Semichem Co.) of ethylene carbonate (EC) and di-methyl carbonate (DMC) with a volume ratio of EC/DMC = 1:1. The electrochemical properties of the assembled cells were recorded with charge/discharge curves in a voltage between 1.0 and 3.0 V vs. Li/Li^+. The CVs were measured using a potentiostat (Eco Chemie, AUTOLAB) at a scan rate of 5 mV s^{-1}. The high rate cycling tests were galvanostatically cycled with varying current densities between 1.0 and 3.0 V vs. Li/Li^+. All of the electrochemical measurements were carried out at 25 ^oC.

3. RESULTS AND DISCUSSION

TEM images of the as-prepared TiO_2@C are shown in Figure 1a and b In the TiO_2@C, the TiO_2 core represented the d-spacing of 0.325 nm corresponding to the {110} facet of the TiO_2 rutile phase whereas the carbon shell displayed the d-spacing of 0.339 nm corresponding to the {002} facet of the graphitic layer. In addition, as indicated in Figure 1c, the TiO_2@C exhibited an average particle size of ~55.7 nm and relatively narrow size distribution. For comparison with TiO_2@C, the TiO_2 sample (TiO_2-800) was prepared by heating commercial TiO_2 powder at 800 ^oC for 3h in air atmosphere for (Figure 1d and e). The average particle size of the TiO_2-800 with a dominant rutile structure was much larger than that of the TiO_2@C (Figure 1f). This shows that the formation of carbon shell at 800 ^oC prevents the aggregation of TiO_2 NPs, thus, resulting in homogeneous graphitic-

like carbon shell and uniform particle size distribution.[7] The graphitic-like carbon shell is formed by the heat treatment process under CH_4 atmosphere. The formation of TiO_2@C nanostructure may take place as equation (2)[42]:

$$TiO_2 + CH_4 \rightarrow TiO_2 + C + 2H_2 \rightarrow TiO_2@C \quad (2)$$

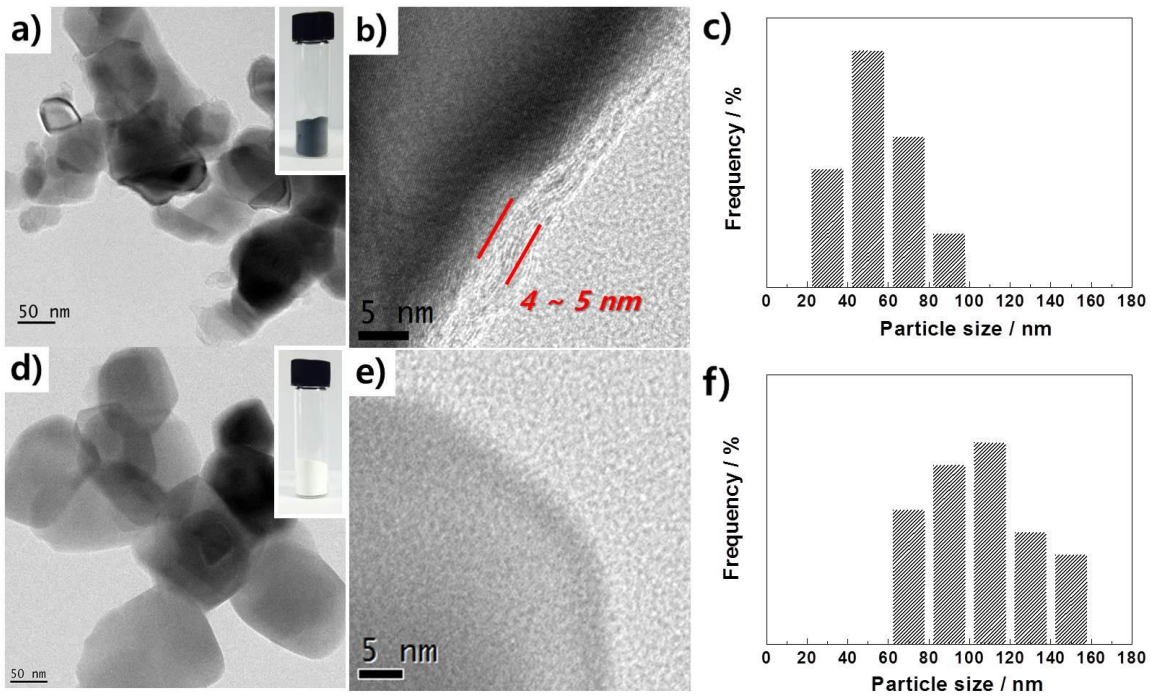

Figure 1. (a) FE-TEM and (b) HR-TEM images, and (c) particle size histogram of the TiO_2@C. (d) FE-TEM and (e) HR-TEM images, and (f) particle size histogram of the TiO_2-800.

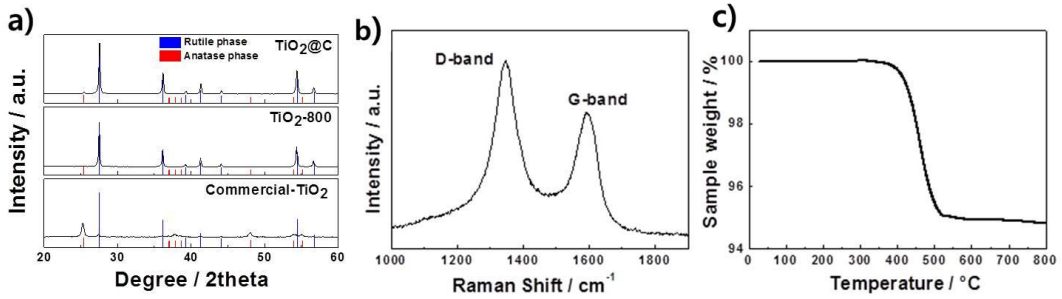

Figure 2. (a) A wide-range XRD pattern of the TiO_2@C, TiO_2-800 and commercial TiO_2 (Degussa, P-25) in comparison with XRD reference data of anatase phase (Red bars, JCPDS No. 89-4921) and rutile phase (Blue bars, JCPDS No. 89-4920) of TiO_2. (b) Raman spectrum of the TiO_2@C nanostructure (c) TGA curve of the TiO_2@C nanostructure in the range of 25–800 ^oC with a heating rate of 10 ^oC min^{-1} in air flow of 60 cm^3 min^{-1}.

The XRD pattern of TiO_2@C showed a dominant rutile phase of TiO_2 with an anatase phase (Figure 2a). Typically, the commercial TiO_2 consists of dominant anatase and rutile phase of TiO_2. In contrast, the annealed TiO_2 samples display mixed phases of anatase and dominant rutile of TiO_2,

which means phase transformation of anatase into rutile phase during heat treatment process in Figure 2a. The anatase phase is transformed into the rutile phase at CH_4 and air atmospheres. In general, it is known that the phase transformation from metastable anatase to stable rutile occurs at ~600 ^oC.[47] The Raman spectrum of the TiO_2@C consisted of two Lorentzian peaks at ~1341 (D-band) and ~1596 cm^{-1} (G-band) caused by defects within the hexagonal graphitic structure and sp^2-hybridized graphitic carbon structures, respectively (Figure 2b). The intensity ratio of D-band to G-band of the TiO_2@C (~0.80) was higher than that of amorphous carbon black (~0.59).[43] Comparing the TEM and Raman data, the TiO_2@C is a well-defined core-shell nanostructure consisting of TiO_2 as a core and graphitic-like carbon as a shell. The amount of carbon in the TiO_2@C nanostructure was determined to be ~5.0 wt% using TGA (Figure 2c). By comparing the TEM, XRD, TGA, and Raman data, the TiO_2@C nanostructure is believed to be well-defined core-shell nanostructures consisting of TiO_2 as a core and graphitic-like carbon as a shell.

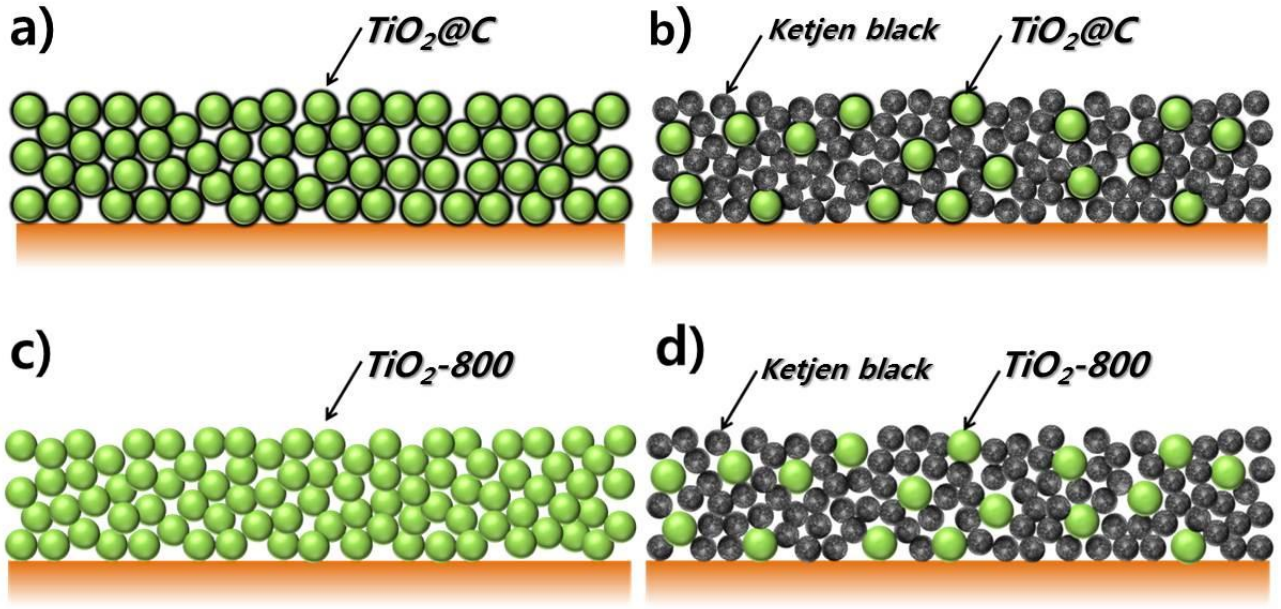

Figure 3. Schematic illustration of electrode structures: (a) f-TiO_2@C, (b) c-TiO_2@C, (c) f-TiO_2-800, and (d) c-TiO_2-800.

The typical anodes for LIBs mainly contained active materials (70 wt%) such as TiO_2@C and TiO_2-800, a binder (20 wt%) such as PVDF and a conducting agent (10 wt%) such as Ketjen Black. In this study, we proposed a conducting agent-free electrode structure (f-TiO_2@C) fabricated using TiO_2@C and PVDF without a conducting agent as illustrated in Figure 3a. For comparison, a conventional electrode structure (c-TiO_2@C) was fabricated using TiO_2@C and PVDF with a conducting agent (Figure 3b). In addition, the conducting agent-free and conventional electrode structures were prepared using TiO_2-800 as an active material (denoted as f-TiO_2-800 (Figure 3c) and c-TiO_2-800 (Figure 3d), respectively).

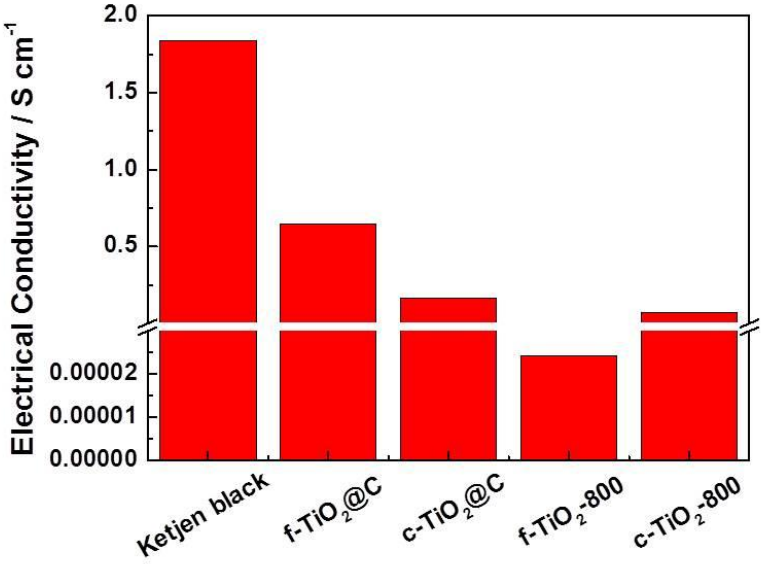

Figure 4. Comparison of electrical conductivity of the as-prepared electrodes.

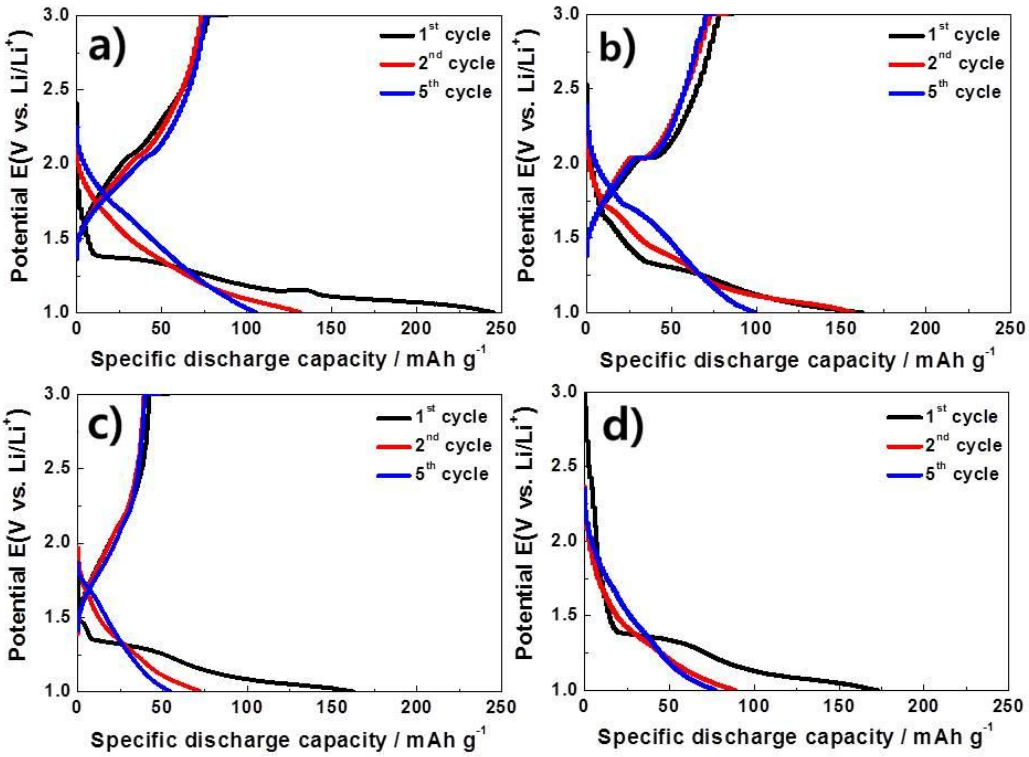

Figure 5. Charge/discharge curves of (a) f-TiO_2@C, (b) c-TiO_2@C, (c) f-TiO_2-800, and (d) c-TiO_2-800 at a current density of 100 mA g^{-1}.

The electrical conductivity of the as-prepared electrodes was compared as shown in Figure 4. The electrical conductivities of c-TiO_2@C and c-TiO_2-800 with Ketjen black as a conducting agent were 0.165 and 0.069 S cm^{-1}, respectively. The f-TiO_2-800 in the absence of a conducting agent

exhibited a relatively low electrical conductivity (2.42×10^{-5} S cm^{-1}). However, it is significant that the f-TiO_2@C as a conducting agent-free electrode holds still higher conductivity (0.65 S cm^{-1}) than the electrodes (c-TiO_2@C and c-TiO_2-800) containing conducting agents. The enhanced conductivity of the f-TiO_2@C may be due to graphitic-like carbon shells, which might play a role as efficient conducting agents for the high-performance LIBs.

Charge/discharge curves of the as-prepared electrodes measured at a current density of 100 mA g^{-1} between 1.0 and 3.0 V in coin-type half-cells are shown in Figure 5a and d. The 1st discharge curves of the electrodes show one plateau region around 1.4 V. The plateau region is attributed to structural rearrangement during the lithium ion intercalation in the rutile phase of TiO_2 structure, from the original rutile (P42/mnm) to its lithiated form (P2/m) at 1.4 V. At a current density of 100 mA g^{-1}, the 1st discharge capacities of the f-TiO_2@C, c-TiO_2@C, f-TiO_2-800, and c-TiO_2-800 were 245.5, 162.3, 162.5, and 172.4 mAh g^{-1}, respectively. The order of capacities of the electrodes was f-TiO_2@C > c-TiO_2@C > c-TiO_2-800 > f-TiO_2-800.[44-46]

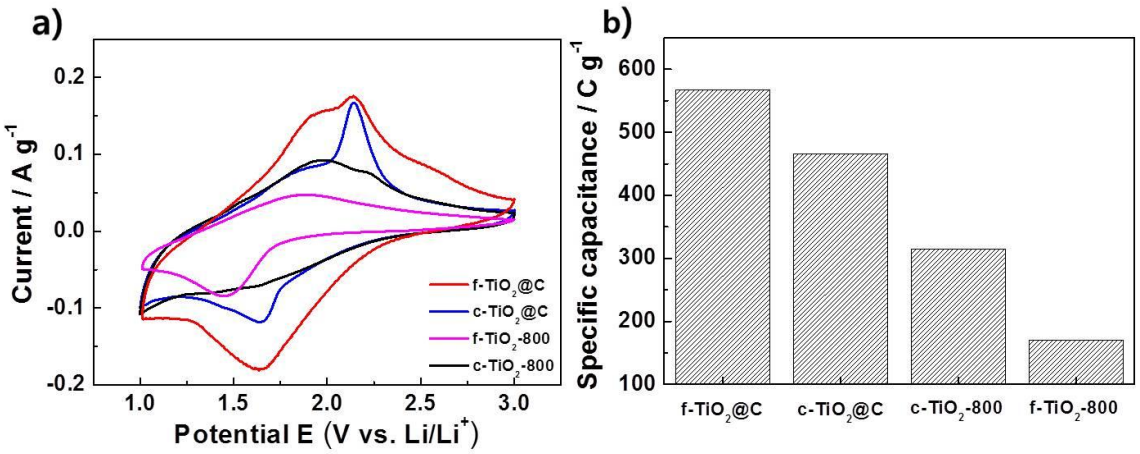

Figure 6. (a) CVs of the electrodes after 5th cycles at a scan rate of 0.5 mV s^{-1}. (b) Specific capacitance of the electrodes at a scan rate of 0.5 mV s^{-1}.

In order to identify electrochemical properties of the f-TiO_2@C, c-TiO_2@C, c-TiO_2-800 and f-TiO_2-800, CVs were obtained after the 5th cycle at a scan rate of 0.5 mV s^{-1} as shown in Figure 6a. The f-TiO_2@C and c-TiO_2@C displayed relatively distinct oxidation and reduction peaks at 2.14 and 1.64 V vs. Li/Li^+, respectively, compared to c-TiO_2-800 and f-TiO_2-800, representing the insertion and desertion of Li^+. Furthermore, among the electrodes, the f-TiO_2@C exhibited the largest CV area i.e., the highest capacitance of ~567.7 C g^{-1} of lithium ion intercalation, indicating the largest discharge capacity (Figure 6b). By comparing the charge/discharge curves and CV data, the improved electrochemical performance of the f-TiO_2@C can be due to graphitic-like carbon shell with a high electrical conductivity.

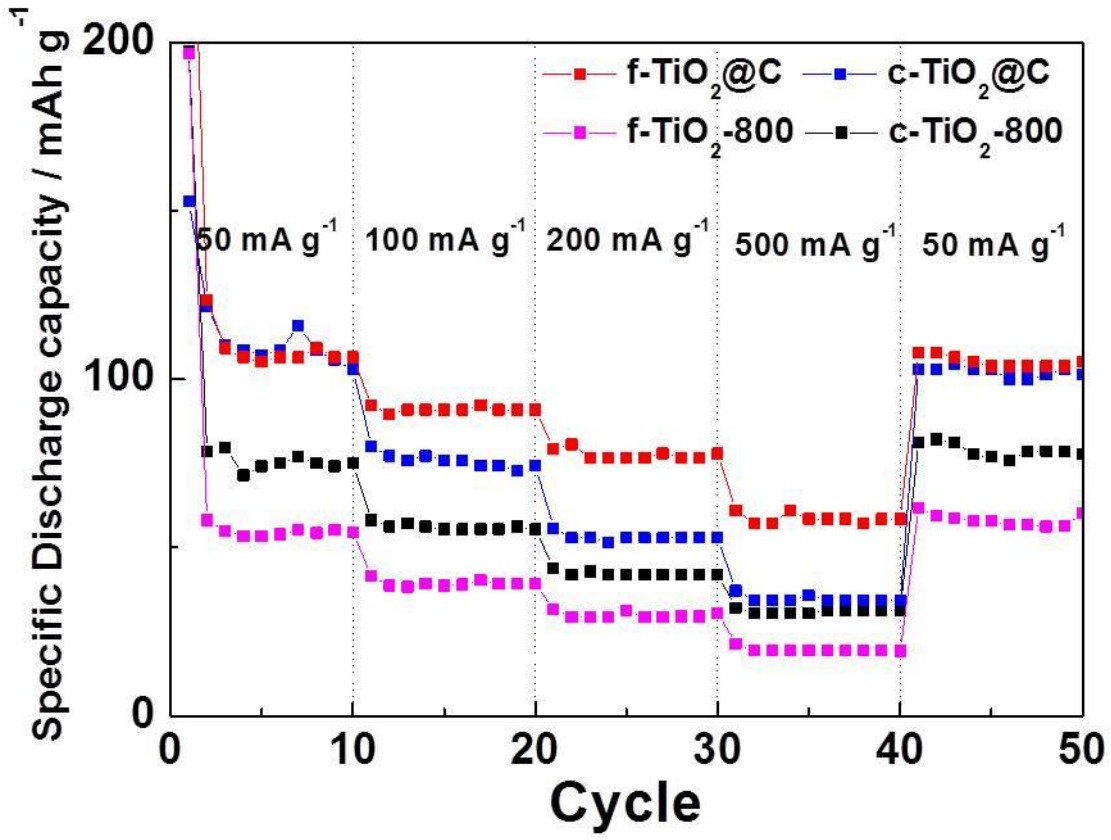

Figure 7. Charge-discharge curves of the electrodes at different C-rates from 50 to 500 mA g^{-1} between 1 and 3 V.

For comparison of the high rate performance of the electrodes, the discharge-charge rates increased from 50 to 500 mA g^{-1}, as indicated in Figure 7. The specific discharge capacities of the f-TiO_2@C, c-TiO_2@C, f-TiO_2-800, and c-TiO_2-800 were 106.5, 102.8, 54.4, and 75 mAh g^{-1} at 50 mA g^{-1}, respectively; 90.9, 74.2, 39.3, and 55.3 mAh g^{-1} at 100 mA g^{-1}, respectively; 77.9, 52.8, 30.5, and 41.9 mAh g^{-1} at 200 mA g^{-1}, respectively; and 58.4, 34.3, 19.1, and 31.3 mAh g^{-1} at 500 mA g^{-1}, respectively. The order of high rate cycling performance of the electrodes was as follows: f-TiO_2@C > c-TiO_2@C > c-TiO_2-800 > f-TiO_2-800. When compared to the cell performance using the TiO_2-800, the c-TiO_2-800 as a conventional electrode with a conducting agent was superior to the f-TiO_2-800 as a conducting agent-free electrode in terms of discharge capacity and high rate cycling behavior. This implies that a conducting agent such as Ketjen black in the electrode structure using a typical active material such as the TiO_2-800 is required for a proper cell performance. On the other hand, in the cells fabricated using the TiO_2@C as an active material, the f-TiO_2@C as a conducting agent-free electrode showed high discharge capacity and excellent high rate cycling performance compared to the c-TiO_2@C as a conventional electrode with a conducting agent. This shows that the graphitic-like carbon shells in the TiO_2@C can play a role as an efficient conducting agent for the high-performance LIBs.

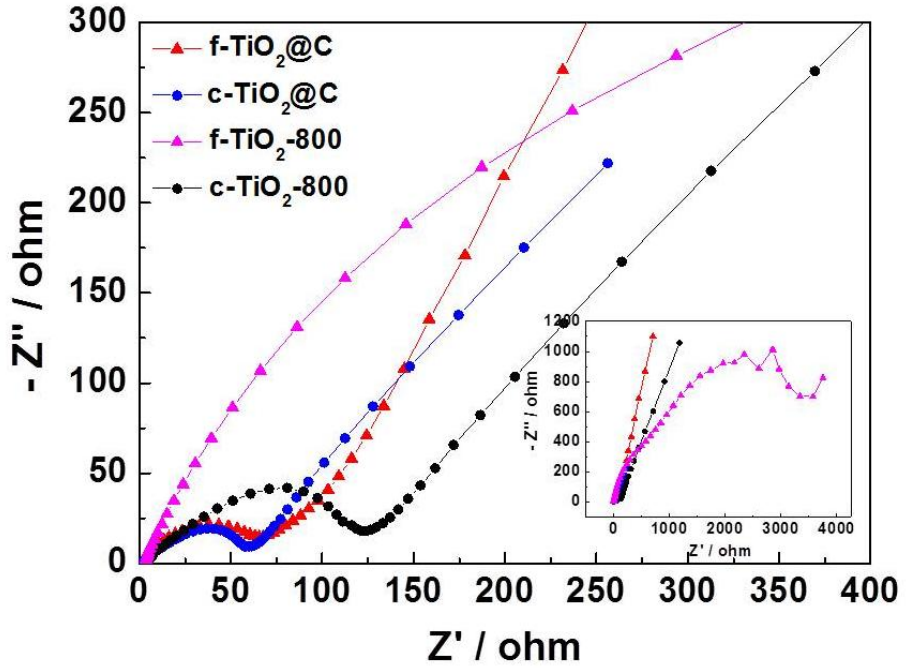

Figure 8. Nyquist plots of impedance data of the electrodes in the frequency ranged between 0.01 Hz and 100 kHz.

To further understand the improved specific discharge capacity of the electrodes, the Nyquist plots were obtained as shown in Figure 8. The value of the diameter of the semicircle on the Z_{real} axis is related to the charge transfer resistance (R_{ct}).[48,49] The values of R_{ct} of the f-TiO_2@C, c-TiO_2@C, f-TiO_2-800, and c-TiO_2-800 were 65.49, 59.31, 4111, 118.6 Ω respectively, representing much enhanced charge transport of the electrodes using the TiO_2@C due to high electrical conductivity. The graphitic-like carbon shell with 4-5 nm thick in the TiO_2@C might improve both electronic and ionic conductivity, thus leading to fast diffusion rate of lithium ion from electrolyte to electrode and low charge transfer resistance.

As shown in the cross sectional SEM images of copper foil, f-TiO_2@C, and c-TiO_2@C (Figure 9), the thickness of the electrodes were ~13.5 μm (f-TiO_2@C) and ~18.8 μm (c-TiO_2@C), respectively. The f-TiO_2@C electrode exhibited ~28.2% reduced thickness in comparison with c-TiO_2@C.

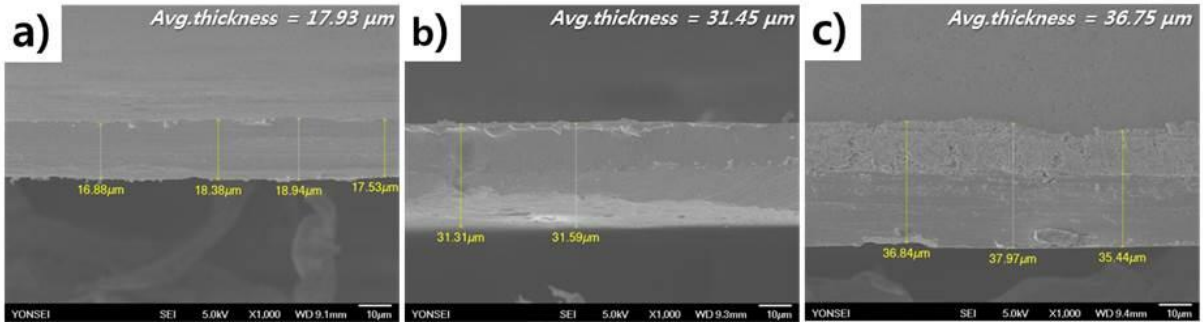

Figure 9. Cross sectional SEM images of (a) copper foil, (b) f-TiO_2@C, and (c) c-TiO_2@C.

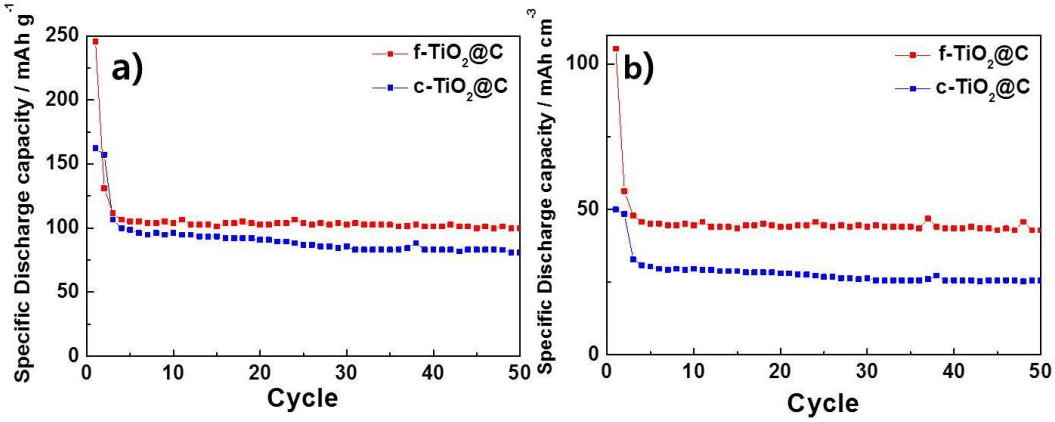

Figure 10. Cycling performance of f-TiO_2@C and c-TiO_2@C at a current rate of 100 mA g^{-1} for 50 cycles: Specific (a) mass and (b) volumetric capacities.

Based on the same amount of anode in the electrodes, the thin f-TiO_2@C demonstrates the conducting agent free-electrode structure with a high packing density, thus resulting in much enhanced volumetric capacity and cycle stability compared to the c-TiO_2@C in the presence of 10 wt% carbon black.

The cycling performance of f-TiO_2@C and c-TiO_2@C at a current rate of 100 mA g^{-1} for 50 cycles is shown in Figure 10. The f-TiO_2@C exhibited much improved performance up to 50 cycles with both reversible specific mass and volumetric capacities of 100 mAh g^{-1} and 42.8 mAh cm^{-3}, respectively, compared with the c-TiO_2@C (81.0 mAh g^{-1} and 25.6 mAh cm^{-3}). The volumetric capacities of the electrodes were calculated from active material area (1.3273 cm^2), and the thickness of the electrodes. The improved cycling performance of the f-TiO_2@C might be mainly attributed to the graphitic-like carbon shell as an efficient conducting agent. This means that, the carbon black contained as a conventional conducting agent in the c-TiO_2@C would not be required for an improved cell performance.

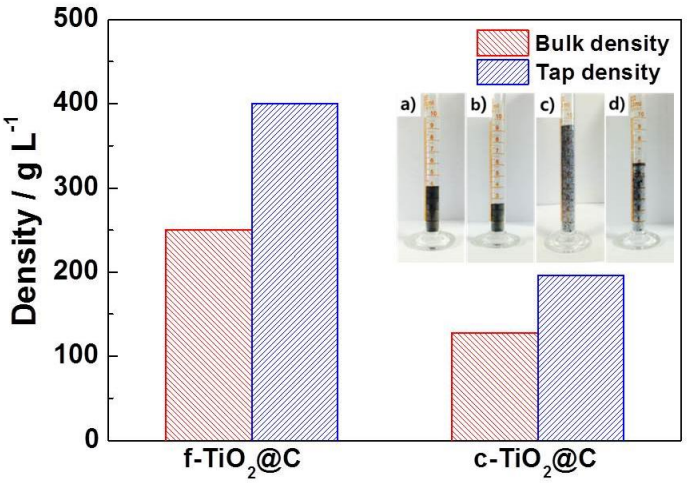

Figure 11. Comparison of bulk density and tapped density of f-TiO_2@C ((a),(b)) and c-TiO_2@C ((c),(d)).

Figure 11 shows comparison of bulk and tap densities of f-TiO_2@C and c-TiO_2@C using the same amount used during the casting step of the electrodes. The f-TiO_2@C exhibited much higher bulk and tap densities of 250 and 400 g L^{-1}, respectively, compared to c-TiO_2@C (128 and 196 g L^{-1}, respectively). In addition, the compressibility of f-TiO_2@C is ~2.9% higher than that of c-TiO_2@C as indicated in Table 1. This means that high bulk and tap densities of f-TiO_2@C might be responsible for high volumetric capacity compared to c-TiO_2@C. As a result, it is concluded that the f-TiO_2@C as a conducting agent free-electrode structure can be an anode candidate for high-performance LIBs.

4. CONCLUSIONS

In summary, we proposed a novel electrode structure without a conducting agent using TiO_2@C with graphitic-like carbon shell, exhibiting an enhanced electrical conductivity. The improved discharge capacity and high rate cycling behavior of the f-TiO_2@C were attributed to the carbon shell in the TiO_2@C, which could play a role as an efficient conducting agent for the high-performance LIBs. Furthermore, the f-TiO_2@C as the conducting agent-free electrode with a high packing density resulted in a high volumetric discharge capacity with an excellent cyclability compared to the c-TiO_2@C in the presence of 10 wt% carbon black as a conducting agent.

ACKNOWLEDGEMENTS
This research was supported by Basic Science Research Program through the National Research Foundation of Korea (NRF) funded by the Ministry of Education (NRF-2013R1A1A2012541)

References

1. J. Cabana, L. Monconduit, D. Larcher and M.-R. Palacin, *Adv. Mater.*, 22 (2010) E170.
2. N. T. H. Trang, Z. Ali and D. J. Kang, *Appl. Mater. Interfaces,* 7 (2015) 3676.
3. B. Dunn, H. Kamath and J.-M. Tarascon, *Science*, .334 (2011) 928.
4. Q. Hao, L. Chen and C. Xu, *Appl. Mater. Interfaces,* 6 (2014) 10107.
5. F. T. Wagner, B. Lakshmanan and M. F. Mathias, *J. Phys. Chem. Lett.*, 1 (2010) 2201.
6. J.-M. Tarascon and M. Armand, *Nature*, 414 (2001) 359.
7. M .K. Song, S. Park, F. M. Alamgir, J. Cho and M. Liu, *Mater. Sci. Eng., R,* 72 (2011) 203.
8. M. C. López, G. F. Ortiz, J. R. González, R. Alcántara and J. L. Tirado, *Appl. Mater. Interfaces,* 6 (2014) 5669.
9. S. J. Kim, Y. W. Lee, S. B. Han, S. B. Kim, W. S. Kim and K. W. Park, *Int. J. Electrochem. Sci.,* 8 (2013) 3825.
10. M. C. Kim, Y. W. Lee, S. J. Kim, B. M. Hwang, H. C. Park, E. T. Hwang, G. Cao and K. W. Park, *Electrochim. Acta*, 147 (2014) 241.
11. W. Wang, Y. Sun, B. Liu, W. Wang and M. Cao, *Carbon*, 91 (2015) 56.
12. M. H. Oh, T. Yu, S. H. Yu, B. Lim, K. T. Ko, M. G. Willinger, D. H. Seo, B. H. Kim, M. G. Cho, J. H. Park, K. Kang, Y. E. Sung, N. Pinna and T. Hyeon, *Science,* 340 (2013) 964.
13. H. Wang, L. F. Cui, Y. Yang, H. S. Casalongue, J. T. Robinson, Y. Liang, Y. Cui and H. Dai, *J. Am. Chem. Soc.*, 132 (2010) 13978.
14. H. Li, T. Zhai, P. He, Y. Wang, E. Hosono and H. Zhou, *J. Mater. Chem.*, 21 (2011) 1780.

15. M. Winter, J. O. Besenhard, M. E. Spahr and P. Novák, *Adv. Mater.*, 10 (1998) 725.
16. M. M. Rahman, J. Z. Wang, M. F. Hassan, D. Wexler and H. K. Liu, *Adv. Energy Mater.*, 1 (2011) 212.
17. H. G. Yang, C. H. Sun, S. Z. Qiao, J. Zou, G. Liu, S. C. Smith, H. M. Cheng and G. Q. Lu, *Nature*, 453 (2008) 638.
18. Z. Yang, D. Choi, S. Kerisit, K. M. Rosso, D. Wang, J. Zhang, G. Graff and J. Liu, *J. Power Sources*, 192 (2009) 588.
19. H. Park, T. Song, H. Han, A. Devadoss, J. Yuh, C. Choi and U. Paik, *Electrochem. Commun.*, 22 (2012) 81.
20. S. Brutti, V. Gentili, H. Menard, B. Scrosati and P. G. Bruce, *Adv. Energy Mater.*, 2 (2012) 322.
21. L. He, C. Wang, X. Yao, R. Ma, H. Wang, P. Chen and K. Zhang, *Carbon*, 75 (2014) 345.
22. D. Wang, D. Choi, Z. Yang. V. V. Viswanathan, Z. Nie, C. Wang, Y. Song, J.-G. Zhang and J. Liu, *Chem. Mater.*, 20 (2008) 3435.
23. B. Han, Y. W. Lee, S. J. Kim, B. M. Hwang, S. B. Kim, W. S. Kim and K. W. Park, *Int. J. Electrochem. Sci.*, 8 (2013) 8264.
24. J. Wang, Y. Zhou, Y. Hu, R. O'Hayre and Z. Shao, *J. Phys.Chem. C*, 115 (2011) 2529.
25. S. J. Kim, Y. W. Lee, B. M. Hwang, S. B. Kim, W. S. Kim, G. Cao and K. Y. Park, *RSC Adv.*, 4 (2014) 11598.
26. J. W. Kang, D. H. Kim, V. Mathew, J. S. Lim, J. H. Gim and J. Kim, *J. Electrochem. Soc.*, 158 (2011) A59.
27. X. Li, Y, Zhou, P. Huang, H. Peng, W. Li, M. Qu, Z. Yu, X. Huang and Y. Chen, *Int. J. Electrochem. Sci.*, 9 (2014) 4816.
28. Q. L. Wu, J. Li, R. D. Deshpande, N. Subramanian, S. E. Rankin, F. Yang and Y.-T. Cheng, *J. Phys. Chem. C*, 116 (2012) 18669.
29. X. Su, Q. L. Wu, X. Zhan, J. Wu, S. Wei and Z. Guo, *J. Mater. Sci.*, 47 (2012) 2519.
30. Z. Yang, Q. Meng, Z. Guo, X. Yu, T. Guo and R. Zeng, *J. Mater. Chem. A*, 1 (2013) 10395.
31. B. Wang, H. Xin, X. Li, J. Cheng, G. Yang and F. Nie, *Sci. Rep.*, 4 (2014) 3729.
32. C. Lai, H. Z. Zhang, G. R. Li and X. P. Gao, *J. Power Sources*, 196 (2011) 4735.
33. C. M. Park, W. S. Chang, H. Jung, J. H. Kim and H. J. Sohn, *Electrochem. Commun.*, 11 (2009) 2165.
34. S.-J. Park, Y.-J. Kim and H. Lee, *J. Power Sources*, 196 (2011) 5133.
35. K.-T. Kim, C.-Y. Yu, S.-J. Kim, Y.-K. Sun and S.-T. Myung, *J. Power Sources*, 281 (2015) 362.
36. C. Kim, R. Buonsanti, R. Yaylian, D. J. Milliron and J. Cabana, *Adv. Energy Mater.*, 3 (2013) 1286.
37. Z. Yang, G. Du, Q. Meng, Z. Guo, X. Yu, Z. Chen, T. Guo and R. Zeng, *J. Mater. Chem.*, 22 (2012) 5848.
38. Z. Yang, G. Du, Z. Guo, X. Yu, Z. Chen, T. Guo and H. Liu, *J. Mater. Chem.*, 21 (2011) 8591.
39. Y. Furuya, W. Zhao, M. Unno and H. Noguchi, *Electrochim. Acta*, 136 (2014) 266.
40. J. Zhang, X. Yan, J. Zhang, W. Cai, X. Wu and Z. Zhang, *J. Power Sources*, 198 (2012) 223.
41. L. Shen, E. Uchaker, C. Yuan, P. Nie, M. Zhang, X. Zhang and G. Cao, *ACS Appl. Mater. Interfaces*, 4 (2012) 2985.
42. J. Ovenstone and K. Yanagisawa, *Chem. Mater.*, 11 (1999) 2770.
43. S. Hussain, R. Amade, E. Jover and E. Bertran, *Nanotechnology*, 23 (2012) 385604.
44. M. Vijayakumar, S. Kerisit, C. Wang, Z. Nie, K. M. Rosso, Z. Yang, G. Graff, J. Liu and J. Hu, *J. Phys. Chem. C*, 113 (2009) 14567.
45. W. J. H. Borghols, M. Wagemaker, U. Lafont, E. M. Kelder and F. M. Mulder, *Chem. Mater.*, 20 (2008) 2949.

46. D. Dambournet, I. Belharouak and K. Amine, *Chem. Mater.*, 22 (2010) 1173.
47. D. A. H. Hanaor and C. C. Sorrell, *J. Mater. Sci.*, 46 (2011) 855.
48. B.-L. He, B. Dong and H.-L. Li, *Eletrochem. Commun.*, 9 (2007) 425.
49. C. Zhao, L. Liu, Q. Zhang, J. Rogers, H. Zhao and Y. Li, *Electrochim. Acta*, 155 (2015) 288.